Journal of the Meteorological Society of Japan

EARLY ONLINE RELEASE

The DOI for this manuscript is

DOI:10.2151/jmsj.2023-017

J-STAGE Advance published date: May 16th, 2023

The final manuscript after publication will replace the preliminary version at the above DOI once it is available.

A hierarchical structure of the heavy rainfall event over Kyushu in July 2020

Hiroki Tsuji[1]

and

Yukari N. Takayabu

Atmosphere and Ocean Research Institute
The University of Tokyo, Tokyo, Japan

April 14, 2023

----

1) Corresponding author: Hiroki Tsuji, Atmosphere and Ocean Research Institute (AORI), The University of Tokyo, Kashiwa, Chiba 277-8568, Japan.

Email: h-tsuji@aori.u-tokyo.ac.jp

Tel: +81-4-7136-4391

Fax: +81-4-7136-4375

Abstract(293/300 words)

The precipitation system and environment causing the heavy rainfall event in July 2020 over Kyushu Island, Japan are analyzed focusing on a hierarchical structure. The moisture budget analysis over Kyushu reveals the contribution of the free-tropospheric moisture flux convergence moistening the atmosphere before the rainfall event. Further analyses by dividing the flux convergence into moisture-advection and wind-convergence terms indicate that the moisture-advection controlled the moistening. Contributions of both the boundary-layer and free-tropospheric wind-convergence terms increase after the moistening. Wide areas with weak precipitation characterize the moistening phase, whereas concentrated intense precipitation areas develop after the moistening. A synoptic scale upper-tropospheric trough transports free-tropospheric moisture from the South China Sea to Kyushu via southern China. The free-tropospheric moisture converges in a sub-synoptic scale cloud system in front of the trough, providing a moist environment favorable for the precipitation systems bringing a large amount of precipitation. A mesoscale depression below the trough developed with active convection over central China enhances the free-tropospheric moisture transport. Cyclonic circulations associated with the mesoscale depression and the sub-synoptic scale cloud system enhance the baroclinicity around Kyushu. An active convective area develops to a mesoscale convective system covering Kyushu under such conditions. A line-shaped convective area is generated along the southern edge of the convective system, causing the heavy rainfall event. Two intense precipitation areas are embedded in the convective area along the inflow direction. At the same time, weak precipitation areas spread downstream of the intense precipitation areas. The vertical cross-sections of the intense precipitation areas show structures consistent with the organized precipitation systems with deep inflow layers and the moist absolutely unstable layers. These results suggest that the organized precipitation system develops under the moist environment prepared by the free-tropospheric moisture flux convergence associated with the hierarchical structure.

Keywords heavy rainfall event; hierarchical structure; mesoscale depression; deep inflow; moist absolutely unstable layer; organized precipitation system

1. **Introduction**

Heavy rainfall events in Japan frequently occur in East Asia summertime monsoon season called Baiu in Japan. In particular, Kyushu Island located in western Japan suffers from disastrous heavy rainfall events in the Baiu season almost every year recently (e.g., Kato et al. 2018; Tsuguti et al. 2018; Shimpo et al. 2019; Araki et al. 2021).

Some previous studies pointed out that the Baiu front, which is a stationary front characterizing the Baiu season, is composed of a hierarchical structure (e.g., Ninomiya and Akiyama 1992). According to Ninomiya and Shibagaki (2003, 2007), a Baiu frontal cloud zone consists of a 2000 km scale cloud system (referred to as a sub-synoptic scale cloud system) and a few meso-alpha-scale cloud systems developed to the trailing portion of the sub-synoptic scale cloud system. They called this hierarchical structure as “a cloud system family”. Within the meso-alpha-scale cloud systems, precipitation systems with more fine-scale structures are confirmed, which cause heavy rainfall events (e.g., Kato 2006). Such hierarchical structure in the Baiu season are confirmed in many rainfall events in the Baiu season (e.g., Akiyama 1989; 1990a, b; Ninomiya 2000; 2020). However, very few studies have discussed the roles and necessity of the hierarchical structure in heavy rainfall events.

Some precipitation systems developed around the Baiu front have similar characteristics to those observed in the tropics (Akiyama 1984a, b; Yokoyama et al. 2014). Akiyama (1978) showed that precipitation systems developed in a Baiu season composed of narrow convective areas and wide stratiform areas, which is similar to tropical mesoscale convective systems (MCSs). Tochimoto and Kawano (2012, 2017a, b) showed that latent heating played a significant role and the baroclinicity contributed less to the development of disturbances developed to the west of 140°E of the Baiu front. Many studies pointed out the significance of latent heating to the development of disturbances on the Baiu front (e.g., Ninomiya and Kurihara 1987; Chang et al. 1998; Ninomiya and Shibagaki 2003; Tagami et al. 2007).

In the tropics, the organization of precipitation systems is a key factor in explaining precipitation amounts. Ahmed and Schumacher (2015) pointed out that the expansion of stratiform precipitation areas associated with organized MCSs explains the relationship between precipitation amount and precipitable water shown by Bretherton et al. (2004). The organization of convection is controlled by free-tropospheric moisture (Sherwood 1999; Kikuchi and Takayabu 2004; Holloway and Neelin 2009). Therefore, moist environments with a large amount of free-tropospheric moisture are a key factor for precipitation amount via the organization of convection.

Organized precipitation systems developed in a moist environment are characterized by deep inflow layers in which air parcels above the cloud bottom flow into convective areas (e.g., Kingsmill and Houze 1999; Houze et al. 2000; Mechem et al. 2002; Parker 2007; Parker and Johnson 2004; Schumacher and Johnson 2008, 2009, Schiro et al. 2018). Bryan and Fritsch (2000) pointed out that moist absolutely unstable layers (MAULs) are generated and maintained by the deep inflow in such MCSs. Organized precipitation systems characterized by the deep inflow and MAUL develop in moderate convective available potential energy (CAPE) and moistened environment (Schumacher and Johnson 2009; Choi et al. 2011). Contrastingly, thunderstorms and supercell storms develop under high convective available potential energy conditions with the dry middle atmosphere (e.g., Gilmore and Wicker 1998; Bluestein and Parker 1993; Zheng et al. 2013).

These contrasting environmental features between MCSs with deep inflow and thunderstorms are consistent with those between precipitation systems bringing the heaviest rainfall and tallest convection (Hamada et al. 2015; Hamada and Takayabu 2018). Hamada and Takayabu (2018) showed that precipitation systems producing a large amount of precipitation in summer around Japan have characteristics of such MCSs. Some previous studies pointed out the significance of the free-tropospheric moisture as a typical environment for heavy precipitation systems around Japan (Unuma and Takemi 2016; Tsuji and Takayabu 2019). These studies indicate that summertime heavy rainfall events in Japan are caused by such mesoscale systems with the deep inflow and MAUL developed under a moist environment.

Recently, Tsuji et al. (2021) statistically showed that free-tropospheric moisture convergence prepares environments favorable for the development of organized precipitation systems with deep inflow and MAUL that cause heavy rainfalls over Kyushu. However, detailed analyses for precipitation systems causing specific heavy rainfall events were a remaining issue because their study was performed regarding area-averaged quantities. Moreover, since they suggested that the preceding increase of the free-tropospheric moisture convergence is associated with a large-scale disturbance, we wanted to examine if an extreme event certainly follows that plot.

In this study, we analyze the preceding moistening and development of the precipitation system causing the rainfall event over Kyushu in July 2020 in terms of a hierarchical structure. In the rainfall event, precipitation amount of over 1000 mm was observed during a week, causing disastrous floods and over 70 fatalities (Hirockawa et al. 2020). We focus on the precipitation system developed on 3–4 July and large-scale environmental features before the development of the precipitation system. Some studies about this case have been performed from various viewpoints (Hirockawa et al. 2020; Araki et al. 2021; Zhao et al. 2021; Horinouchi et al. 2021; Taylor et al. 2021; Tochimoto et al. 2022; Kitabatake et al. 2022; Kawano and Kawamura 2022). However, analyses focusing on the hierarchical structure and their role in developing the precipitation system have not been performed. In the rest of this paper, we explain the data and method used in this study in section 2. The results are presented in section 3. The summary of this paper is shown in section 4 with some discussions.

2. Data and Method

2.1 Data

The three-hourly initial values of the Japan Meteorological Agency (JMA) operational

Mesoscale Model (MSM; JMA, 2019) are used to investigate the moisture budget and the environment around the rainfall area. These data have 16 vertical layers and a horizontal resolution of 0.125° longitude × 0.1° latitude, covering a region of 120°E–150°E, 22.4°N–47.6°N. The MSM produced precipitation data (initial values) with a horizontal resolution of 0.0625° longitude × 0.05° latitude are also used.

Six-hourly Japanese 55-year global atmospheric reanalysis (JRA55) product (Kobayashi et al. 2015) with a 1.25° × 1.25° horizontal resolution and 37 vertical layers are used to investigate the synoptic environment before the event including outside of the MSM product coverage.

Infrared (10.4 μm) brightness temperature distribution observed by the Himawari-8 geostationary satellite (Yamamoto et al. 2020; Takenaka et al. 2020) and precipitation data estimated from the JMA operational weather radar data (Japan Meteorological Agency observations department 2004) are used to identify cloud systems found during the analysis period. Horizontal resolutions of these data are 0.02° and 1 km, respectively.

2.2 Methodology

We evaluate the time evolutions of each term of the moisture budget equation in the Kyushu region (30°N–35°N, 128.75°E–132.5°E, Fig. 1) calculated with the MSM data, as in Tsuji et al. (2021). The moisture budget equation is as follows:

$$\frac{\partial \mathrm{PW}}{\partial t} = \frac{1}{g}\int_{p1}^{p2}(-\nabla \cdot q\vec{v})dp - \mathrm{P} + \mathrm{E},$$

where PW, t, g, q, $\vec{v}$, p, p_1, p_2, P, and E denote precipitable water, time, gravity acceleration, mixing ratio, horizontal wind, pressure, 1000 hPa, 300 hPa, precipitation, and evaporation, respectively. We ignore evaporation due to its small contribution around Kyushu to total rainfall in the rainfall event (Zhao et al. 2021). Vertically integrated water vapor flux convergences (hereafter, IVFCs) are calculated by integrating water vapor flux convergences at each layer. We also calculate free-tropospheric IVFC by integration in the 900–300 hPa layer and boundary-layer IVFC by integration in the 1000–900 hPa layer to evaluate the roles of the IVFC in each layer, as in Tsuji et al. (2021).

The IVFC is further divided into a wind-convergence term and an advection term as follows:

$$\frac{1}{g}\int_{p1}^{p2}(-\nabla\cdot q\vec{v})dp = \frac{1}{g}\int_{p_1}^{p_2}(-q\nabla\cdot\vec{v})dp + \frac{1}{g}\int_{p_1}^{p_2}(-\vec{v}\cdot\nabla q)dp.$$

The wind-convergence term (the first term of the RHS) is calculated with the same method as the IVFC. The advection term (the second term of the RHS) is obtained as the residual.

The MAUL condition is defined following Takemi and Unuma (2020) as

$$\text{RH} > 99\% \text{ and } \frac{\partial\theta_e}{\partial z} < 0,$$

where RH, θ_e, and z, are the relative humidity, equivalent potential temperature, and height, respectively. Takemi and Unuma (2020) set this definition after considering potential errors in moisture representations in the MSM and pointed out that the definition is stricter than that used in Bryan and Fritsch (2000). The equivalent potential temperature is calculated from temperature, pressure, mixing ratio, and water vapor pressure using Bolton's (1980) method. The water vapor pressure is calculated using saturation water pressure calculated with Huang's (2018) method and relative humidity.

In section 3.2, we show the two-dimensional frontogenesis function (Petterssen 1936) defined as follows:

$$F = \frac{1}{|\nabla\theta|}\left[\frac{\partial\theta}{\partial x}\left(-\frac{\partial u}{\partial x}\frac{\partial\theta}{\partial x} - \frac{\partial v}{\partial x}\frac{\partial\theta}{\partial y}\right) + \frac{\partial\theta}{\partial y}\left(-\frac{\partial u}{\partial y}\frac{\partial\theta}{\partial x} - \frac{\partial v}{\partial y}\frac{\partial\theta}{\partial y}\right)\right],$$

where θ, x, y, u, and v designate the potential temperature, eastward coordinate, northward coordinate, zonal wind component and meridional wind component, respectively.

3. Results

In this section, we first show the time evolutions of each term of the moisture budget equation calculated over the Kyushu region (section 3.1). We also show time evolutions of rainfall area coverages and moisture. Based on the analyses of the time evolutions, we divide the rainfall event into two periods: Period I, when the atmosphere is moistened before the rainfall event, and Period II, when the precipitation system causing the rainfall event develops. The analyses focusing on the large-scale environment moistening the atmosphere in Period I are shown in section 3.2. In section 3.3, analyses of the characteristics of the precipitation system developed under the moist environment in Period II are shown.

3.1 Time evolutions over the Kyushu region

Figure 2a shows the time evolution of each term in the moisture budget equation.

Maximum area-averaged precipitation during the rainfall event is detected at 03 JST (JST=UTC+9) 4 July (hereafter, referred to as the rainfall peak time). The free-tropospheric IVFC starts to be positive at 06 JST 2 July and reaches its maximum at 12 JST 3 July, before the rainfall peak time. Until 15 JST 3 July, the free-tropospheric IVFC has a larger value compared to the boundary-layer IVFC (Fig. 2a). The change in the free-tropospheric IVFC is characterized by the advection term until 00 JST 3 July, while the contribution of wind-convergence term increases after 00 JST 3 July (Fig. 2b). The evolution of the precipitable water tendency follows that in the free-tropospheric advection (Fig. 2b). The boundary-layer IVFC starts to be positive at 15 JST 2 July, nine hours later than the free-tropospheric IVFC (Fig. 2a). The change in the boundary-layer IVFC is mainly associated with the wind-convergence term and the advection term contributes less to the total IVFC throughout the analysis period. The difference in the contribution of the two terms between the boundary-layer and free-tropospheric IVFCs causes the delay in the onset time of the boundary-layer IVFC. The free-tropospheric IVFC begins to increase by the advection of large-scale circulation, whereas the boundary-layer IVFC begins to increase by the wind-convergence term in association with convections developed in the moist environment provided by the free-tropospheric IVFC. The wind-convergence term in both the boundary-layer and free-troposphere is dominant around the rainfall peak time. The onset times of these terms are close to each other (18 and 21 JST 2 July, respectively) as well as those for their maximum values (03 and 06 JST 4 July). The amplitudes of the wind-convergence terms are comparable. These results indicate that the free-tropospheric advection contributes to moistening the atmosphere before the rainfall peak time. After the moistening, the precipitation system causing the rainfall event develops with convergence in a deep layer.

A remarkable moistening is observed at 500–600 hPa from 06 JST 2 July to 15 JST 3 July (Fig. 3). In this layer, relative humidity increases to over 70%. The mixing ratio increases fourfold. The increasing period corresponds to that of the positive precipitable water tendency and positive free-tropospheric IVFC (Fig. 2a). After 15 JST 3 July, the mid-tropospheric moisture starts to decrease. In contrast, the boundary-layer moisture continues to increase after 15 JST 3 July and reaches its maximum at 03 JST 4 July. However, the increase speed of the boundary-layer moisture is slower than that in the free troposphere.

Figure 4 shows time evolutions of rainfall area coverages obtained from the JMA operational weather radar data for four different precipitation thresholds. Before 18 JST 3 July, wide rainfall areas with weak precipitation intensity cover Kyushu. Most rainfall areas consist of precipitation weaker than 5 mm h^{-1}. However, after 18 JST 3 July, weaker rainfall areas shrink, whereas intense rainfall area coverages increase. In particular, rainfall areas over 30 mm h^{-1} expanded after 18 JST 3 July. The change in the rainfall area characteristics indicates a transition of precipitation systems bringing rainfall to the Kyushu region.

These results indicate that this rainfall event consists of two periods: In the first period (Period I: 09 JST 2 July to 15 JST 3 July), the atmosphere is moistened primarily by the free-tropospheric advection with weak precipitation. We analyze this part in section 3.2 focusing on the synoptic environment that moistens the atmosphere over the Kyushu region. In the second period (Period II: 18 JST 3 July to 03 JST 4 July), the wind-convergence terms play a significant role in generating the precipitation system with intense precipitation under moistened environments. We analyze the second part focusing on the characteristics of the precipitation system causing the heavy rainfall event that developed under the moistened environment in section 3.3.

3.2 Synoptic environment moistening the atmosphere over the Kyushu region

To reveal the processes moistening the atmosphere before the rainfall event by the free-tropospheric IVFC, we investigate synoptic conditions in Period I. At 09 JST 2 July, a synoptic scale upper-tropospheric trough starts to develop over central China (around 110°E, Fig. 5a). Active convection with brightness temperature lower than 220 K develops near the trough (around 30°N, 110°E at Fig. 6a). A local maximum of 850 hPa vorticity collocates with the active convection (Fig. 7a, labeled as Y). The free-tropospheric moisture flux comes from the South China Sea toward this trough. The free-tropospheric IVFC is analyzed over a 2000 km scale area in front of the trough (110°E–130°E, 25°N–35°N, Fig. 5a). A brightness temperature lower than 260 K characterizes this area (Fig. 6a) with a vorticity maximum at 500 hPa (Fig. 7a, labeled as A). Because these characteristics are similar to those of the sub-synoptic scale cloud system shown in Ninomiya and Shibagaki (2003; 2007), this 2000 km scale area is defined as a sub-synoptic scale cloud system.

The upper-tropospheric trough develops as propagates eastward (Figs. 5b–5d). Below the trough, a positive vorticity area with about a 1000 km scale is analyzed in association with a mesoscale depression (Figs. 7b-7d, labeled as B for 500 hPa and Y for 850 hPa). The free-tropospheric moisture flux is enhanced to the southeast of the mesoscale depression with developing the trough and depression, which also enhances the free-tropospheric IVFC in the sub-synoptic scale cloud system (Figs. 5b–5d). A large gradient of precipitable water is analyzed in the Kyushu region at 21 JST 2 July (Fig. 5b), contributing to generating the large value of the free-tropospheric moisture advection (Fig. 2b). After this time, the Kyushu region is covered by an area with precipitable water over 50 mm (Figs. 5c and 5d), comparable to the tropics. The free-tropospheric moisture flux comes to the Kyushu region from the South China Sea via southern China located to the south of the trough during Period I (Fig. 5). These results indicate that the moisture transport associated with the synoptic scale upper-tropospheric trough, enhanced by the mesoscale depression, and converged in the sub-synoptic scale cloud system, plays a significant role in moistening the Kyushu region before the rainfall peak time.

With the eastward propagation of the trough, the sub-synoptic scale cloud system also propagated eastward (Figs. 6b–6d) with the vorticity maximum at 500 hPa (Fig. 7b–7d, labeled as A). The maximum value of over 6×10^{-5} s^{-1} sustains during Period I although a few other local maxima appear around the maximum. A vorticity maximum of over 6×10^{-5} s^{-1} at 850 hPa is analyzed to the south of the 500 hPa vorticity maximum in the sub-synoptic scale cloud area at 09 JST 2 July (Fig. 7a, labeled as X), propagating eastward with development (Figs. 7b-7d). As the upper-tropospheric trough develops, the vorticity maximum associated with the mesoscale depression develops at 500 and 850 hPa (Figs. 7b–7d, labeled as B for 500 hPa and Y for 850 hPa). At 15 JST 3 July, the maximum values reach over 1×10^{-4} s^{-1} and locate over the East China Sea (Fig. 7d).

To investigate the environment around the Kyushu region, Fig. 8 shows temperature, wind vector, and horizontal temperature advection at 850 hPa obtained from the JRA55 data from 09 JST 3 July to 03 JST 4 July. Westerly or southwesterly winds are enhanced in a wide area around the Kyushu region (125°E–145°E, 30°N–35°N) by circulations associated with the sub-synoptic scale cloud system and the mesoscale depression. In association with the warm advection by the southwesterly winds, the temperature to the south of Kyushu increases over 2 K from 09 JST 3 July to 03 JST 4 July. To the north of Kyushu around 36°N, easterly winds are analyzed in association with the cyclonic circulation of these systems (Fig. 8) and an anti-cyclonic circulation of the high-pressure system centered around 42°N, 135°E. Temperature around 36°N decreases by over 2 K from 09 JST 3 July to 03 JST 4 July. The horizontal distribution of temperature advection (contours) indicates that the horizontal temperature advection does not contribute to this temperature decrease. Some physical processes such as nighttime radiative cooling from the surface under clear sky may be contributing. A detailed discussion about the mechanism of the temperature decrease is left for future work.

These temperature tendencies enhance the baroclinicity around the Kyushu region in Period II. Figure 9 shows the horizontal temperature gradient and two-dimensional frontogenesis function at 850 hPa calculated with JRA55 data. A small temperature gradient is analyzed at 09 JST 3 July (Fig. 9a) around the Kyushu region. A positive frontogenesis region collocates with the mesoscale depression in the East China Sea. In contrast, the sub-synoptic scale cloud system has a smaller temperature gradient compared to the mesoscale depression. As the circulations are enhanced, areas with large temperature gradients and positive frontogenesis expand horizontally. At 21 JST 3 July and 03 JST 4 July, a frontogenesis region is analyzed in the north part of the Kyushu region (Fig. 9c, 9d). Ninomiya and Shibagaki (2003) pointed out that the increase in the baroclinicity plays a role in the sub-synoptic scale cloud system to prepare the environment favorable for active convection at the trailing portion of the cloud system. Kitabatake et al. (2022) suggested that the ascending forcing associated with the enhancement of the front in this baroclinic field can initiate active convections at the beginning of the heavy rainfall.

3.3 Characteristics of a precipitation system causing the rainfall event

In this subsection, we focus on the characteristics of a precipitation system developed under the moist environment prepared in Period I. Figure 10 shows snapshots of IR images and precipitation distribution for a precipitation system causing the heavy rainfall event. An active convective area with a brightness temperature lower than 200 K is generated to the west of Kyushu (32°N, 129°E) at 18 JST 3 July (Fig. 10a). This convective area develops into an MCS with a horizontal scale of a few hundred kilometers at the rainfall peak time (Fig. 10d). A meso-beta-scale line-shaped narrow area with intense precipitation of over 80 mm h^{-1} is observed along the south edge of the MCS at 00 JST 4 July (Fig. 10g, 128°E–133°E, 32°N–32.5°N). The area is also identified at 03 JST 4 July, causing the disastrous rainfall event (Fig. 10h). A wide area with weak precipitation is observed around the north and west of the line-shaped narrow area (Fig. 10h). Such precipitation distribution is similar to that associated with an organized MCS consisting of narrow intense convective areas and wide stratiform precipitation areas (e.g., Houze 2004).

The MSM precipitation product reasonably reproduces the precipitation distribution around the rainfall peak time although precipitation intensity is weaker than the observation (Fig. 11). Two intense precipitation areas with precipitation over 40 mm h^{-1} are distributed along the water vapor flux in both 00 JST and 03 JST 4 July (around 129°E and 131°E, Fig. 11), which are embedded in the line-shaped narrow area. A wide area with precipitation weaker than 20 mm h^{-1} is distributed to the north and east of the intense precipitation area. Because of westerly winds in the middle to upper troposphere over the Kyushu region (not shown), the wide weak precipitation area locates on the downstream side of the intense precipitation areas. MAULs are analyzed around the intense precipitation areas.

To investigate detailed structures of the intense precipitation areas, we make vertical cross-sections along with the vertically integrated water vapor flux (Fig. 12). Inflow layers deeper than the boundary layer slantly ascend around the intense precipitation areas (32°N–32.3°N) at 03 JST 4 July for the two cross-sections. MAUL conditions are satisfied around the ascending area. Such distributions of wind, equivalent potential temperature, and MAULs are similar to the idealized schematic figure of MCS with deep inflow and MAUL shown by Bryan and Fritch (2000). The slantwise ascending inflow layer is also observed at 00 JST 4 July in the eastern intense precipitation area (Fig. 12c). Although the slantwise ascent of the inflow layer is unclear in the western intense precipitation area at 00 JST 4 July (Fig. 12a), the low-level winds tend to ascend at around 31.8°N. Additionally, some grids with MAUL conditions are observed. These results indicate that the deep inflow layer with MAUL sustains a few hours around the MCS.

4. Summary, Conclusions, and Discussions

4.1 Summary

A case study of a heavy rainfall event in July 2020 over Kyushu, Japan is conducted focusing on a hierarchical structure associated with the environmental conditions which moisten the atmosphere before the rainfall event and the characteristics of the precipitation system causing the heavy rainfall. The hierarchical structure is schematically shown in Fig. 13a. The water vapor budget analysis over the Kyushu region reveals that the precipitable water tendency increases following the change in the free-tropospheric moisture advection till 9 hours before the rainfall event (Period I). Weak precipitation is observed over a wide area in the Kyushu region. After the moistening, wind-convergence terms in both boundary-layer and free-troposphere become dominant (Period II). The precipitation area in Period II shrinks compared to that in Period I, but areas with intense precipitation expand. The moistening in Period I is caused by a convergence of southwesterly moisture flux associated with a synoptic scale upper-tropospheric trough. The convergence area locates in front of the trough with a sub-synoptic scale (about 2000 km scale) cloud system. The upper-tropospheric trough develops by active convection over central China accompanied by a mesoscale (about 1000 km scale) depression in the lower troposphere. The mesoscale depression enhances southwesterly moisture flux, helping to further moisten the atmosphere in the sub-synoptic scale cloud system. Then, the Kyushu region is covered by an area with precipitable water over 50 mm, comparable to the tropics, by these moistening processes. In Period II, a cyclonic circulation associated with the sub-synoptic scale cloud system and the mesoscale depression increases baroclinicity around the Kyushu region in the lower troposphere. The moist environment and baroclinicity help to generate an MCS at the trailing portion of the sub-synoptic scale cloud system. A meso-beta-scale precipitation area extending west-east directions develops at the southern edge of the MCS, causing the heavy rainfall event. At the same time, slantly ascending deep inflow layers with MAULs are diagnosed in the intense precipitation area (Fig. 13b). The characteristics of the MCS are consistent with the organized precipitation system.

4.2 Conclusions and Discussions

The results of the analyses indicate that the rainfall event is characterized by a hierarchical structure such that the organized precipitation system with meso-beta-scale intense precipitation areas develops under the moist environment and baroclinicity generated by the upper-tropospheric trough, the sub-synoptic scale cloud system and the mesoscale depression. The organized precipitation system causing the disastrous rainfall event develops with deep inflow and MAUL under the moist environment provided by the free-tropospheric IVFC associated with large-scale features. Therefore, studies of large-scale environmental features as well as fine-scale features of the precipitation systems causing heavy rainfall events are significant to understand the generation and development of the precipitation systems.

The results of this study emphasize the significance of the moistening in the free troposphere before the rainfall event. The moist environment in the free troposphere is favorable for the development of the organized precipitation systems with deep inflow and MAUL (e.g., Bryan and Fritch 2000; Mechem et al. 2002). Such organized precipitation systems bring about intense precipitation (Hamada et al. 2015; Hamada and Takayabu 2018). A large amount of free tropospheric moisture is also confirmed in some case studies about rainfall events in Japan (Hirota et al. 2016; Takemi and Unuma 2019; Tsuji et al. 2020; Yokoyama et al. 2020; Unuma and Takemi 2021). Moreover, the increases in the free-tropospheric IVFC and precipitable water tendency before rainfall events are shown statistically by Tsuji et al. (2021). We show that the preceding moistening is associated with an upper tropospheric trough, a sub-synoptic scale cloud system, and a mesoscale depression. The sub-synoptic scale cloud system passing before the heavy rainfall event is consistent with the concept of the cloud system family (Ninomiya and Shibagaki 2003; 2007). Some previous studies indicate that upper tropospheric troughs play a role to develop mesoscale disturbances and rainfall events over East Asia (Nie and Fan 2019: Shibuya et al. 2021). Tochimoto et al. (2022) pointed out that the upper tropospheric trough affects the development of the mesoscale depression and moisture flux to the Kyushu region in this event. Our results and these previous studies suggest that such large-scale conditions can be used as a key factor to predict heavy rainfalls.

In this study, the detailed processes of the development of the precipitation system, such as how the inflow layer ascent develops, is not investigated. The orography of Kyushu can contribute to lifting the deep inflow layer and producing MAUL in part of the precipitation area developed over Kyushu (Fig. 10), as suggested by Takemi and Unuma (2020). However, the intense precipitation area is also developed over the ocean (Fig. 10). Some previous studies about the organized precipitation systems suggest that a mesoscale circulation produced by a gravity wave response to a quasi-steady diabatic heating associated with convection generates the slantwise ascent (e.g., Pandya and Durran 1996; Fovell 2002; Liu and Moncrieff 2017). For the precipitation system in this event, Kitabatake et al. (2022) pointed out the significance of the lower tropospheric baroclinicity, mid-tropospheric dry air advection, and dynamical forcing associated with the upper tropospheric trough to the development of the precipitation system can cause the rainfall event. Further quantitative studies about what factors contribute to the development are needed.

Although this study suggests that the moist environment and organized precipitation system with deep inflow and MAUL are key factors for rainfall events, some previous studies also identified rainfall events that are caused by other factors. For example, extremely tall convections are observed in a heavy rainfall event in July 2017 in northern Kyushu (Kato et al. 2018). Some studies pointed out that the characteristics of the precipitation system causing rainfall events are consistent with those in the extreme convections of Hamada and Takayabu (2018) (Tsuji et al. 2020, Sato et al. 2021). Moreover, Ito et al. (2020) pointed out that MAULs hardly contributed to the precipitation system causing the heavy rainfall event in northern Kyushu in 2017. For rainfall events with such the extreme convection type systems, convective instability associated with boundary-layer moisture transport and mid-level dry air may play a significant role to produce the precipitation systems causing rainfall events (e.g., Kato and Goda 2001; Tsuguti and Kato 2014; Kato 2006, 2018, 2020). Further studies are needed to clarify conditions that determine the characteristics of precipitation systems.

Data Availability Statement

The MSM products were obtained from the database of Research Institute for Sustainable

Humanosphere, Kyoto University. The JRA55 products were provided by JMA. Himawari 8 gridded data are distributed by Center for Environmental Remote Sensing (CEReS), Chiba University, Japan. These are available at following URLs:

MSM: http://database.rish.kyoto-u.ac.jp/arch/jmadata/data/gpv/original/

JMA operational weather radar: http://database.rish.kyoto-u.ac.jp/arch/jmadata/data/jma-radar/synthetic/original/

JRA55: https://jra.kishou.go.jp/JRA-55/index_en.html

Himawari 8: http://www.cr.chiba-u.jp/databases/GEO/H8_9/FD/index.html

Acknowledgments

This research is supported by Japan Aerospace Exploration Agency (JAXA) Precipitation Measuring Mission science, the University of Tokyo through a project “Research hub for the big data analysis of global water cycle and precipitation in changing climate”, and the Environment Research and Technology Development Fund (JPMEERF20222002) of the Environmental Restoration and Conservation Agency Provided by the Ministry of Environment of Japan. The MSM products and the JMA operational weather radar data were obtained from the database of Research Institute for Sustainable Humanosphere, Kyoto University. Himawari 8/9 gridded data are distributed by the Center for Environmental Remote Sensing (CEReS), Chiba University, Japan.

References

Ahmed, F., and C. Schumacher, 2015: Convective and stratiform components of the precipitation-moisture relationship. *Geophys. Res. Lett.*, **42**, 10,453–10,462, doi:10.1002/2015GL066957.

Akiyama, T. 1978: Mesoscale pulsation of convective rain in medium-scale disturbances developed in Baiu front. *J. Meteor. Soc. Japan*, **62**, 267–283, https://doi.org/10.2151/jmsj1965.56.4_267

Akiyama, T., 1984a: A medium-scale cloud cluster in a Baiu front Part I: Evolution process and fine structure. *J. Meteor. Soc. Japan*, **62**, 485–504, doi: 10.2151/jmsj1965.62.3_485.

Akiyama, T., 1984b: A medium-scale cloud cluster in a Baiu front Part II: Thermal and kinematic fields and heat budget. *J. Meteor. Soc. Japan*, **62**, 505–521, doi: 10.2151/jmsj1965.62.3_505.

Akiyama, T., 1989: Large, synoptic and meso scale variations of the Baiu front, during July 1982 Part I: Cloud features. *J. Meteor. Soc. Japan*, **67**, 57–81, https://doi.org/10.2151/jmsj1965.67.1_57.

Akiyama, T., 1990a: Large, synoptic and meso scale variations of the Baiu front, during July 1982 Part II: Frontal Structure and Disturbances. *J. Meteor. Soc. Japan*, **68**, 557–574, https://doi.org/10.2151/jmsj1965.68.5_557.

Akiyama, T., 1990b: Large, synoptic and meso scale variations of the Baiu front, during

July 1982 Part III: Space-time scale and structure of frontal disturbances. *J. Meteor. Soc. Japan*, **68**, 705–727, https://doi.org/10.2151/jmsj1965.68.6_705.

Araki, K., T. Kato, Y. Hirockawa, and W. Mashiko, 2021: Characteristics of atmospheric environments of quasi-stationary convective bands in Kyushu, Japan during the July 2020 heavy rainfall event. *SOLA*, **17**, 8−15, doi:10.2151/sola.2021-002.

Bluestein, H. B., and S. S. Parker, 1993: Modes of isolated, severe convective storm formation along the dryline. *Mon. Wea. Rev.*, **121**, 1354–1372, doi:10.1175/1520-0493(1993)121<1354:MOISCS>2.0.CO;2

Bolton, D. (1980): The computation of equivalent potential temperature. *Mon. Wea. Rev.*, **108**, 1046–1053, doi.org:10.1175/1520-0493(1980)108<1046:TCOEPT>2.0.CO;2

Bretherton, C. S., M. E. Peters, and L. E. Back. 2004: Relationship between water vapor path and precipitation over the tropical oceans. *J. Climate,* **17**, 1517–1528, doi: 10.1175/1520-0442(2004)017<1517:RBWVPA>2.0.CO;2

Bryan, G. H., and J. M. Fritsch, 2000: Moist absolute instability: The sixth static stability state. *Bull. Amer. Meteor. Soc.*, **81**, 1207–1230, doi:10.1175/1520-0477(2000)081<1287:MAITSS>2.3.CO;2.

Chang, C.-P., S. C. Hou, H. C. Kuo, and G. T. J. Chen, 1998: The development of an intense East Asian summer monsoon disturbance with strong vertical coupling. *Mon. Wea. Rev.*, **126**, 2692–2712, doi: 10.1175/1520-0493(1998)126<2692:TDOAIE>2.0.CO;2.

Choi, H.-Y., J.-H. Ha, D.-K Lee, and Y.-H. Kuo, 2011: Analysis and simulation of mesoscale convective systems accompanying heavy rainfall: The Goyang case. *Asia-Pacific J. Atmos. Sci.*, 47, 265–279, doi:10.1007/s13143-011-0015-x.

Fovell, R. G., 2002: Upstream influence of numerically simulated squall-line storms. *Quart. J. Roy. Meteor. Soc.*, **128**, 893–912, doi:10.1256/0035900021643737.

Gilmore, M. S., and L. J. Wicker, 1998: The influence of midtropospheric dryness on supercell morphology and evolution. *Mon. Wea. Rev.*, **126**, 943–958, doi:10.1175/1520-0493(1998)126<0943:TIOMDO>2.0.CO;2.

Hamada, A., and Y. N. Takayabu, 2018: Large-scale environmental conditions related to midsummer extreme rainfall events around Japan in the TRMM region. *J. Climate*, **31**, 6933–6945, doi:10.1175/JCLI-D-17-0632.1.

Hamada, A., Y. N. Takayabu, C. Liu, and E. J. Zipser, 2015: Weak linkage between the heaviest rainfall and tallest storms. *Nat. Commun.*, **6**, 6213, doi:10.1038/ncomms7213.

Hirockawa, Y., T. Kato, K. Araki, and W. Mashiko, 2020: Characteristics of an extreme rainfall event in Kyushu district, southwestern Japan in early July 2020. *SOLA*, **16**, 265–270, doi:10.2151/sola.2020-044.

Hirota, N., Y. N. Takayabu, M. Kato, and S. Arakane, 2016: Roles of an atmospheric river and a cutoff low in the extreme precipitation event in Hiroshima on 19 August 2014. *Mon. Wea. Rev.*, **144**, 1145–1160, doi:10.1175/MWR-D-15-0299.1.

Holloway, C. E., and J. D. Neelin, 2009: Moisture vertical structure, column water vapor, and tropical deep convection. *J. Atmos. Sci.*, **66**, 1665–1683, doi: 10.1175/2008JAS2806.1.

Horinouchi, T., Y. Kosaka, H. Nakamigawa, H. Nakamura, N. Fujikawa, and Y. N. Takayabu, 2021: Moisture supply, jet, and Silk-Road wave train associated with the prolonged heavy rainfall in Kyushu, Japan in early July 2020. *SOLA*, **17B**, 1−8, doi:10.2151/sola.2021-019.

Houze Jr., R. A., 2004: Mesoscale convective systems. *Rev. Geophys.*, **42**, RG4003, doi:10.1029/2004RG000150.

Houze Jr., R. A., S. S. Chen, D. E. Kingsmill, Y. Serra, and S. E. Yuter, 2000: Convection over the Pacific warm pool in relation to the atmospheric Kelvin-Rossby wave. *J. Atmos. Sci.*, **57**, 3058–3089, doi:10.1175/1520-0469(2000)057<3058:COTPWP>2.0.CO;2.

Huang, J., 2018: A simple accurate formula for calculating saturation vapor pressure of water and ice. *J. Appl. Meteor. Climatol.*, **57**, 1265–1272. Doi.org:10.1175/JAMC-D-17-0334.1

Ito, J., H. Tsuguchi, S. Hayashi, and H. Niino, 2021: Idealized high-resolution simulations of a back-building convective system that causes torrential rain. *J. Atmos. Sci*, **78**, 117–132, doi:10.1175/JAS-D-19-0150.1.

Japan Meteorological Agency, 2019: Outline of the operational numerical weather prediction at the Japan Meteorological Agency. (Available online at: https://www.jma.go.jp/jma/jma-eng/jma-center/nwp/outline2019-nwp/index.htm, accessed 23 February 2022)

Japan Meteorological Agency Observations Department, 2004: 1 km mesh zenkoku gousei radar GPV no teikyoutou ni tsuite (Data provision of nationwide composited radar grid point value with 1 km resolutions). Technical Information, No. 162, 28 pp (in Japanese). (Available at https://www.data.jma.go.jp/add/suishin/ jyouhou/pdf/162.pdf, accessed 23 February 2022)

Kato, R., S. Shimizu, K. Shimose, T. Maesaka, N. Sakurai, and Y. Shusse, 2018: Prompt report of meteorological analysis on the July 2017 Northern Kyushu Heavy Rainfall. *Natural Disaster Research Report of the National Research Institute for Earth Science and Disaster Resilience*, No. 52, 7 pp. (in Japanese).

Kato, T., 2006: Structure of the band-shaped precipitation system inducing the heavy rainfall observed over northern Kyushu, Japan on 29 June 1999. *J. Meteor. Soc. Japan*, **84**, 129–153, doi:10.2151/jmsj.84.129.

Kato, T., 2018: Representative height of the low-level water vapor field for examining the initiation of moist convection leading to heavy rainfall in East Asia. *J. Meteor. Soc. Japan*, **96**, 69–83, doi:10.2151/jmsj.2018-008.

Kato, T., 2020: Quasi-stationary band-shaped precipitation systems, named “Senjo-Kousuitai”, causing localized heavy rainfall in Japan. *J. Meteor. Soc. Japan*, **98**, 485–

509, doi:10.2151/jmsj.2020-029.

Kato, T., and H. Goda, 2001: Formation and maintenance processes of a stationary band-shaped heavy rainfall observed in Niigata on 4 August 1998. *J. Meteor. Soc. Japan*, **79**, 899–924, doi:10.2151/jmsj.79.899.

Kawano, T., and R. Kawamura, 2022: Remote effect of Kuroshio warm SSTs in the East China Sea on heavy rainfall in southern Kyushu, Japan on 3 July 2020. *SOLA*, in press, https://doi.org/10.2151/sola.2022-033

Kikuchi, K., and Y. N. Takayabu, 2004: The development of organized convection associated with the MJO during TOGA COARE IOP: Trimodal characteristics, *Geophys. Res. Lett.*, **31**, L10101, doi:10.1029/2004GL019601.

Kingsmill, D. E., and R. A. Houze Jr., 1999: Thermodynamic characteristics of air flowing into and out of precipitating convection over the west Pacific warm pool. *Quart. J. Roy. Meteor. Soc.*, **125**, 1209–1229, doi:10.1002/qj.1999.49712555606.

Kitabatake, N., S. Makino, Y. Iwashita, T. Ito, and T. Kato, 2022: effects of synoptic–scale environments on the Baiu frontal heavy rainfall event in Kumamoto prefecture on 3–4 July 2020. *Tenki*, **69**, 87–99, https://doi.org/10.24761/tenki.69.2_87. (in Japanese)

Kobayashi, S., Y. Ota, Y. Harada, A. Ebita, M. Moriya, H. Onoda, K. Onogi, H. Kamahori, C. Kobayashi, H. Endo, K. Miyaoka, and K. Takahashi, 2015: The JRA-55 Reanalysis: General specifications and basic characteristics. *J. Meteor. Soc. Japan*, **93**, 5–48, doi:10.2151/jmsj.2015-001.

Liu, C., and M. W. Moncrieff 2017: Shear-parallel mesoscale convective systems in a moist low-inhibition Mei-yu front environment. *J. Atmos. Sci.*, **74**, 4213–4228, doi:10.1175/JAS-D-17-0121.1.

Mechem, D. B., R. A. Houze Jr., and S. S. Chen, 2002: Layer inflow into precipitating convection over the western tropical Pacific. *Quart. J. Roy. Meteor. Soc.*, **128**, 1997–2030, doi: 10.1256/003590002320603502.

Nie, J., and B. Fan, 2019: Roles of dynamic forcings and diabatic heating in summer extreme precipitation in east China and the southeastern United States. *J. Climate,* **32**, 5815–5831, https://doi.org/10.1175/JCLI-D-19-0188.1.

Ninomiya, K, 2000: Large- and meso-α-scale characteristics of Meiyu/Baiu front associated with intense rainfalls in 1-10 July 1991. *J. Meteor. Soc. Japan*, **78**, 141–157, https://doi.org/10.2151/jmsj1965.78.2_141.

Ninomiya, K, 2020: Variations of Baiu frontal cloud–precipitation systems over Japan observed in July 1982. *Tenki*, **67**, 331–342, https://doi.org/10.24761/tenki.67.6_331. (in Japanese)

Ninomiya, K, and T. Akiyama, 1992: Multi-scale features of Baiu, the summer monsoon over Japan and the East Asia. *J. Meteor. Soc. Japan*, **70**, 467–495, https://doi.org/10.2151/jmsj1965.70.1B_467.

Ninomiya, K., and K. Kurihara, 1987: Forecast experiment of a long-lived meso-α-scale convective system in Baiu frontal zone. *J. Meteor. Soc. Japan*, **65**, 885–899, doi:10.2151/jmsj1965.65.6_885.

Ninomiya, K., and Y. Shibagaki, 2003: Cloud system families in the Meiyu-Baiu front observed during 1-10 July 1991. *J. Meteor. Soc. Japan*, **81**, 193–209, doi: 10.2151/jmsj.81.193.

Ninomiya, K., and Y. Shibagaki, 2007: Multi-scale features of the Meiyu-Baiu front and associated precipitation systems. *J. Meteor. Soc. Japan*, **85B**, 103–122, doi: 10.2151/jmsj.85B.103.

Pandya R. E., and D. R. Durran, 1996: The influence of convectively generated thermal forcing on the mesoscale circulation around squall lines. *J. Atmos. Sci.*, **53**, 2924–2951, doi:10.1175/1520-0469(1996)053<2924:TIOCGT>2.0.CO;2.

Parker, M. D., 2007: Simulated convective lines with parallel stratiform precipitation. Part I: An archetype for convection in along-line shear. *J. Atmos. Sci.*, **64**, 267–288, doi:10.1175/JAS3853.1.

Parker, M. D., and R. H. Johnson, 2004: Simulated convective lines with leading precipitation. Part II: Evolution and maintenance. *J. Atmos. Sci.*, **61**, 1656–1673, doi:10.1175/1520-0469(2004)061<1656:SCLWLP>2.0.CO;2.

Petterssen, S., 1936: Contribution to the theory of frontogenesis. *Geofys. Publ.*, **11**, 1-27.

Sato, Y., S. Hayashi, and A. Hashimoto, 2021: Difference in the lightning frequency between the July 2018 heavy rainfall event over central Japan and the 2017 northern Kyushu heavy rainfall event in Japan. *Atmos. Sci. Lett.*, **23**, e1067, doi.org/10.1002/asl.1067.

Schiro, K. A., F. Ahmed, S. E. Giangrande, and J. D. Neelin, 2018: GoAmazon2014/5 campaign points to deep-inflow approach to deep convection across scales. *Proc. Natl. Acad. Sci. USA*, **115**, 4577–4582, https://doi.org/10.1073/pnas.1719842115.

Schumacher, R. S., and R. H. Johnson, 2008: Mesoscale processes contributing to extreme rainfall in a midlatitude warm-season flash flood. *Mon. Wea. Rev.*, **136**, 3964–3986, doi:10.1175/2008MWR2471.1.

Schumacher, R. S., and R. H. Johnson, 2009: Quasi-stationary, extreme-rain-producing convective systems associated with midlevel cyclonic circulations. *Wea. Forecasting*, **24**, 555–574, doi:10.1175/2008WAF2222173.1.

Sherwood, S. C., 1999: Convective precursors and predictability in the tropical western Pacific. *Mon. Wea. Rev.*, **127**(12), 2977–2991, doi:10.1175/1520-0493(1999)127<2977:CPAPIT>2.0.CO;2.

Shibuya, R, Y. N. Takayabu, and H. Kamahori, 2021: Dynamics of widespread extreme precipitation events and the associated large-scale environment using AMeDAS and JRA-55 data. *J. Climate,* **34**, 8955–8970, https://doi.org/10.1175/JCLI-D-21-0064.1.

Shimpo, A., K. Takemura, S. Wakamatsu, H. Togawa, Y. Mochizuki, M. Takekawa, S. Tanaka, K. Yamashita, S. Maeda, R. Kurora, H. Murai, N. Kitabatake, H. Tsuguti, H. Mukougawa, T. Iwasaki, R. Kawamura, M. Kimoto, I. Takayabu, Y. N. Takayabu, Y. Tanimoto, T. Hirooka, Y. Masumoto, M. Watanabe, K. Tsuboki, and H. Nakamura, 2019: Primary factors behind the Heavy Rainfall Event of July 2018 and the subsequent heat wave in Japan. *SOLA*, **15A**, 13–18, https://doi.org/10.2151/sola.15A-003.

Tagami, H., H. Niino, and T. Kato, 2007: A Study of meso-α-scale disturbances on the Baiu front and their environmental field. *J. Meteor. Soc. Japan*, **85**, 767–784, https://doi.org/10.2151/jmsj.85.767.

Takemi, T., and T. Unuma, 2019: Diagnosing environmental properties of the July 2018 heavy rainfall event in Japan. *SOLA*, **15A**, 60−65, https://doi.org/10.2151/sola.15A-011.

Takemi, T., and T. Unuma, 2020: Environmental factors for the development of heavy rainfall in the eastern part of Japan during Typhoon Hagibis (2019). *SOLA*, **16**, 30−36, doi:10.2151/sola.2020-006.

Takenaka, H., T. Sakashita, A. Higuchi, T. Nakajima, 2020: Development of geolocation correction for geostationary satellite observation by phase only correlation method using visible channel, *Remote Sens.*, **12**, 2472, doi:10.3390/rs12152472.

Taylor, J., A. Amemiya, T. Honda, Y. Maejima, and T. Miyoshi, 2021: Predictability of the July 2020 heavy rainfall with the SCALE-LETKF. *SOLA*, **17**, 48−56, doi:10.2151/sola.2021-008.

Tochimoto, E., and T. Kawano, 2012: Development processes of Baiu frontal depressions. *SOLA*, **8**, 9–12, doi: 10.2151/sola.2012-003.

Tochimoto, E., and T. Kawano, 2017a: Numerical Investigation of Development Processes of Baiu Frontal Depressions Part I: Case Studies. *J. Meteor. Soc. Japan*, **95**, 91–109, doi:10.2151/jmsj.2017-005.

Tochimoto, E., and T. Kawano, 2017b: Numerical Investigation of Development Processes of Baiu Frontal Depressions Part II: An Idealized Study. *J. Meteor. Soc. Japan*, **95**, 217–237, doi:10.2151/jmsj.2017-012.

Tochimoto, E., S. Iizuka, and T. Ohigashi, 2022: Influence of an upper-level trough on the formation of a baiu frontal depression that caused a torrential rainfall event in southern Kyushu, Japan on July 4, 2020. *SOLA*, **18A**, 1−7, doi:10.2151/sola.18A-001.

Tsuguti, H., and T. Kato, 2014: Contributing factors of the heavy rainfall event at Amami-Oshima Island, Japan, on 20 October 2010. *J. Meteor. Soc. Japan*, **92**, 163– 183, doi:10.2151/jmsj.2014-202.

Tsuguti, H., N. Seino, H. Kawase, Y. Imada, T. Nakaegawa, and I. Takayabu, 2018: Meteorological overview and mesoscale characteristics of the Heavy Rain Event of July 2018 in Japan. *Landslides*, **16**, 363–371, https://doi.org/10.1007/s10346-018-1098-6.

Tsuji, H., and Y. N. Takayabu, 2019: Precipitation enhancement via the interplay between atmospheric rivers and cutoff lows. *Mon. Wea. Rev.*, **147**, 2451–2466, doi:10.1175/MWR-D-18-0358.1.

Tsuji, H., C. Yokoyama, and Y. N. Takayabu, 2020: Contrasting features of the July 2018 heavy rainfall event and the 2017 northern Kyushu rainfall event in Japan. *J. Meteor. Soc. Japan*, **98**, 859–876, doi:10.2151/jmsj.2020-045.

Tsuji, H., Y. N. Takayabu, R. Shibuya, H. Kamahori, and C. Yokoyama, 2021: The role of free-tropospheric moisture convergence for summertime heavy rainfall in western Japan. *Geophys. Res. Lett.*, **48**, e2021GL095030, doi:10.1029/2021GL095030.

Unuma, T., and T. Takemi, 2016: Characteristics and environmental conditions of quasi-stationary convective clusters during the warm season in Japan. *Quart. J. Roy. Meteor. Soc.*, **142**, 1232–1249, doi:10.1002/qj.2726.

Unuma, T., and T. Takemi, 2021: Rainfall characteristics and their environmental conditions during the heavy rainfall events over Japan in July of 2017 and 2018. *J. Meteor. Soc. Japan*, **99**, 165–180, doi:10.2151/jmsj.2021-009.

Yamamoto, Y., K. Ichii, A. Higuchi, and H. Takenaka, 2020: Geolocation correction for geostationary satellite observations by a phase-only correlation method using a visible channel. *Remote Sens.*, **12**, doi:10.3390/rs12152472.

Yokoyama, C., Y. N. Takayabu, and S. Kanada, 2014: A contrast in precipitation characteristics across the Baiu front near Japan. Part I: TRMM PR observation. *J. Climate,* **27**, 5872–5890, doi:10.1175/JCLI-D-13-00350.1.

Yokoyama, C., H. Tsuji, and Y. N. Takayabu, 2020: The effects of an upper-tropospheric trough on the heavy rainfall event in July 2018 over Japan, *J. Meteor. Soc. Japan*, **98**, 235–255, doi:10.2151/jmsj.2020-013.

Zhao, N., A. Manda, X. Guo, K. Kikuchi, T. Nasuno, M. Nakano, Y. Zhang, and B. Wang, 2021: A Lagrangian view of moisture transport related to the heavy rainfall of July 2020 in Japan: Importance of the moistening over the subtropical regions, *Geophys. Res. Lett.*, **48**, e2020GL091441, doi:10.1029/2020GL091441.

Zheng, L., J. Sun, X. Zhang, and C. Liu, 2013: Organizational modes of mesoscale convective systems over central East China. *Wea. Forecasting*, **28**, 1081–1098, doi:10.1175/WAF-D-12-00088.1.

List of Figures

Fig. 1. A map around the analysis region. The red rectangle designates the Kyushu region.

Fig. 2. (a) Time evolution of the total IVFC (black, bold), boundary-layer IVFC (red with triangle marks), free-tropospheric IVFC (blue with cross marks), precipitation (purple), and precipitable water tendency (green, dotted line) (units: mm day^{-1}) in the heavy rainfall event in July 2020. The abscissa designates local time (UTC + 9). (b) Same as in Fig. 2a, but for the boundary-layer advection (red, bold), boundary-layer wind-convergence (red, thin), free-tropospheric advection (blue, bold), and free-tropospheric wind-convergence (blue, thin). Precipitation (purple) and precipitable water tendency (green, dotted line) are also plotted.

Fig. 3: Time-height cross-section of relative humidity (color, %) and mixing ratio (contour g kg^{-1}) averaged over the Kyushu area obtained from the MSM data. The ordinate and

abscissa designate pressure (hPa) and local time (UTC + 9), respectively.

Fig. 4: (a) Time evolution of area coverages of precipitation (km2) more than 1 mm h^{-1} (black), 5 mm h^{-1} (green), 10 mm h^{-1} (blue), and 30 mm h^{-1} (red) within the Kyushu area calculated with JMA operational radar data. The abscissa designates local time (UTC + 9).

Fig. 5: Horizontal distributions of the free-tropospheric IVFC (color, mm day^{-1}), precipitable water (red contour, mm, shown only over 40 mm), free-tropospheric moisture flux (vector, kg m^{-1} s^{-1}, shown only over 200 kg m^{-1} s^{-1}), and isentropic potential vorticity on 350 K (green contour, shown only 1, 2, and 3 PVU) obtained from JRA55 data at (a) 09 JST 2 July, (b) 21 JST 2 July, (c) 09 JST 3 July, and (d) 15 JST 3 July.

Fig. 6: (a) Infrared brightness temperature (K) observed by Himawari 8 at (a) 09 JST 2 July, (b) 21 JST 2 July, (c) 09JST 3 July, and (d) 15 JST 3 July.

Fig. 7: Relative vorticity at 500 hPa (color, $\times 10^{-5}$ s^{-1}) and 850 hPa (black contours, $\times 10^{-5}$ s^{-1}) obtained from JRA55 data at (a) 09 JST 2 July, (b) 21 JST 2 July, (c) 09 JST 3 July, and (d) 15 JST 3 July. Only positive values are shown. Blue contours designate potential vorticity on 350 K isentropic surface (PVU, shown only 1, 2, and 3 PVU contours).

Fig. 8: Temperature (color, °C), wind vectors (m s^{-1}, shown only over 2.5 m s^{-1}), and horizontal temperature advection (contours, $-V \cdot \nabla T$, 10^{-5} K s^{-1}) at 850 hPa obtained from JRA55 data at (a) 09 JST 3 July, (b) 15 JST 3 July, (c) 21 JST 3 July, and (d) 03 JST 4 July. The contour intervals are 1×10^{-5} K s^{-1} for the cold advection and 5×10^{-5} K

s^{-1} for the warm advection.

Fig. 9: (a–d) Infrared brightness temperature (K) observed by Himawari 8 and (e–h) precipitation distribution observed by JMA weather radar (mm h^{-1}) at (a, e) 18 JST 3 July, (b, f) 21 JST 3 July, (c, g) 00 JST 4 July, and (d, h) 03 JST 4 July.

Fig. 10: Horizontal temperature gradient [color, K (100 km)$^{-1}$] and horizontal frontogenesis [K (100 km)$^{-1}$ (day)$^{-1}$, shown only over 0.5 K (100 km)$^{-1}$ (day)$^{-1}$] at 850 hPa calculated with JRA55 data at (a) 09 JST 3 July, (b) 15 JST 3 July, (c) 21 JST 3 July, and (d) 03 JST 4 July.

Fig. 11: Precipitation distribution (color, mm h^{-1}) and vertically (1000–300 hPa) integrated water vapor flux (vector, kg m^{-1} s^{-1}, shown only over 1000 kg m^{-1} s^{-1}) obtained from the MSM data at (a) at 00 JST 4 July and (b) at 03 JST 4 July. Orange contours designate areas where MAUL conditions are satisfied at least 2 vertical levels between 500 and 800 hPa. Green dashed lines mark the location of the cross-sectional analyses in Fig. 12.

Fig. 12: Vertical cross-sections of a wind velocity along the cross-section (color, m s^{-1}), wind vectors (arrow, m s^{-1} for horizontal direction and Pa s^{-1} for vertical direction), and equivalent potential temperature (black contour, K) along the green dashed lines in Fig. 10 at (a, c) 00 JST 4 July and (b, d) 03 JST 4 July. The black circles indicate grids that fulfill the MAUL condition. The ordinate designates pressure (hPa).

Fig. 13: Schematics of (a) the hierarchical structure characterizing the heavy rainfall event,

and (b) Vertical structure of the organized precipitation system. Note that MAUL designate moist absolutely unstable layer.

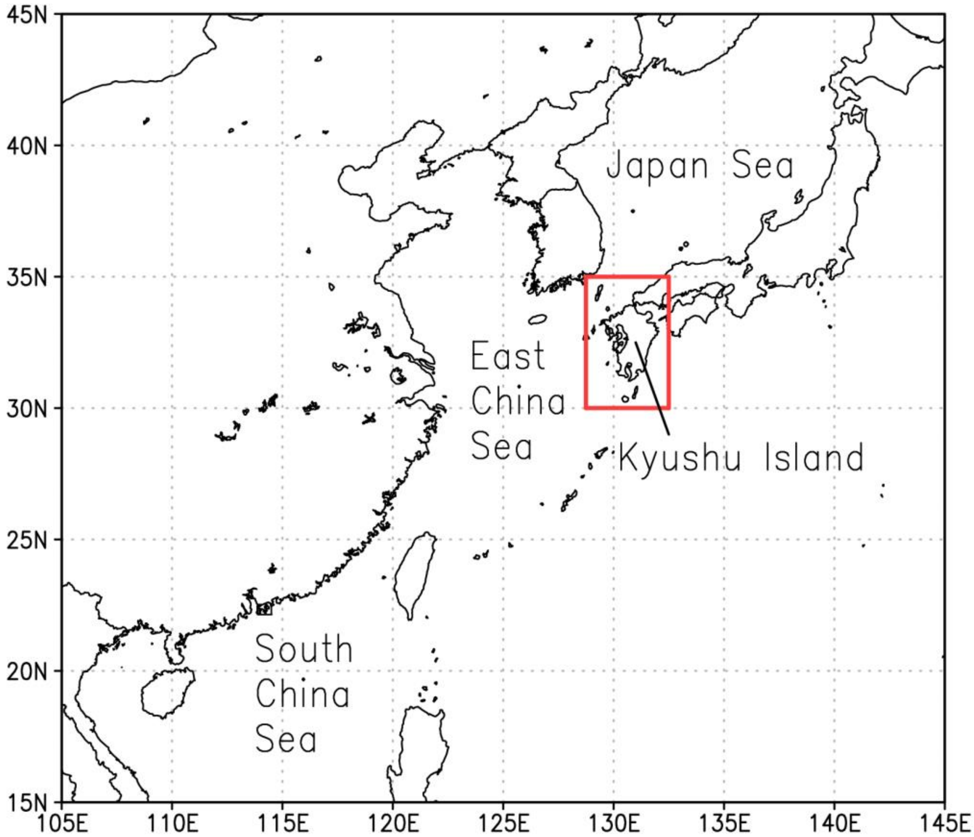

Fig. 1 A map around the analysis region. The red rectangle designates the Kyushu region.

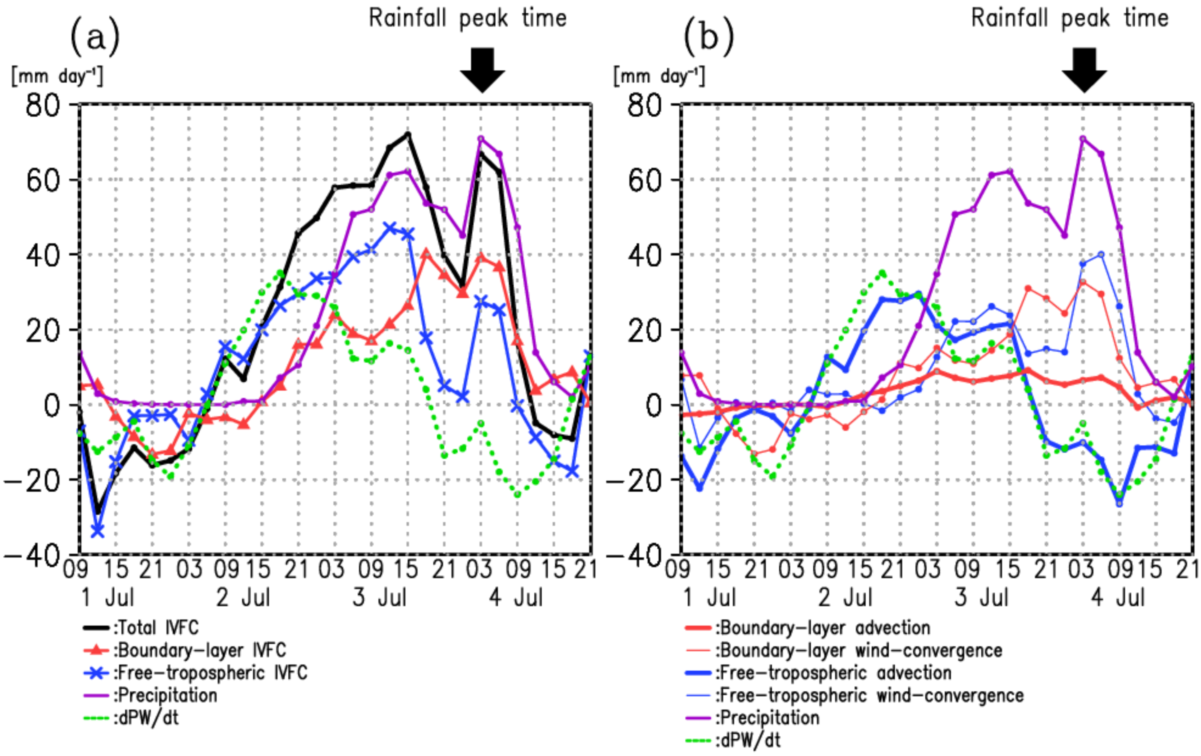

Fig. 2 (a) Evolution of the total IVFC (black, bold), boundary-layer IVFC (red with triangle marks), free-tropospheric IVFC (blue with cross marks), precipitation (purple), and precipitable water tendency (green, dotted line) (units: mm day^{-1}) in the heavy rainfall event in July 2020. The abscissa designates local time (UTC + 9). (b) Same as in Fig. 2a, but for the boundary-layer advection (red, bold), boundary-layer wind-convergence (red, thin), free-tropospheric advection (blue, bold), and free-tropospheric wind-convergence (blue, thin). Precipitation (purple) and precipitable water tendency (green, dotted line) are also plotted.

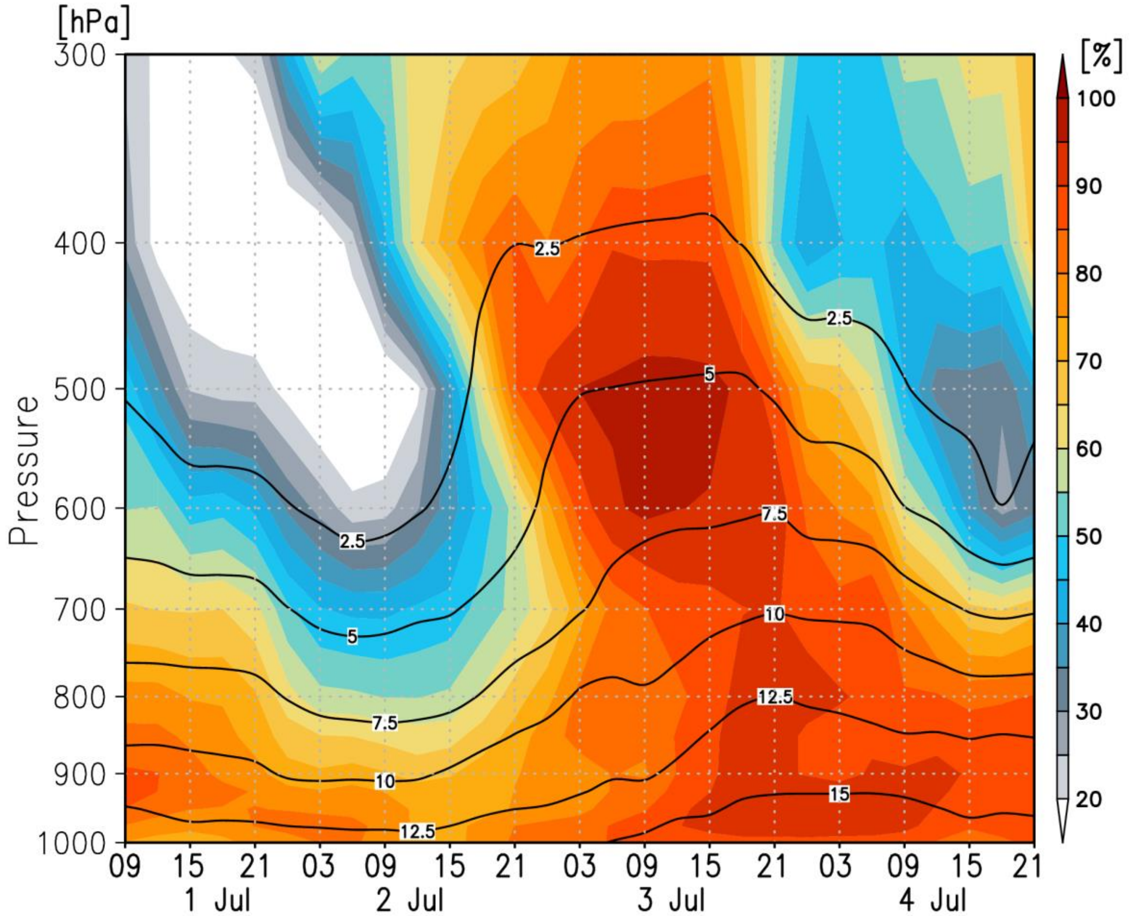

Fig. 3 Time-height cross-section of relative humidity (color, %) and mixing ratio (contour g kg^{-1}) averaged over the Kyushu area obtained from the MSM data. The ordinate and abscissa designate pressure (hPa) and local time (UTC + 9), respectively.

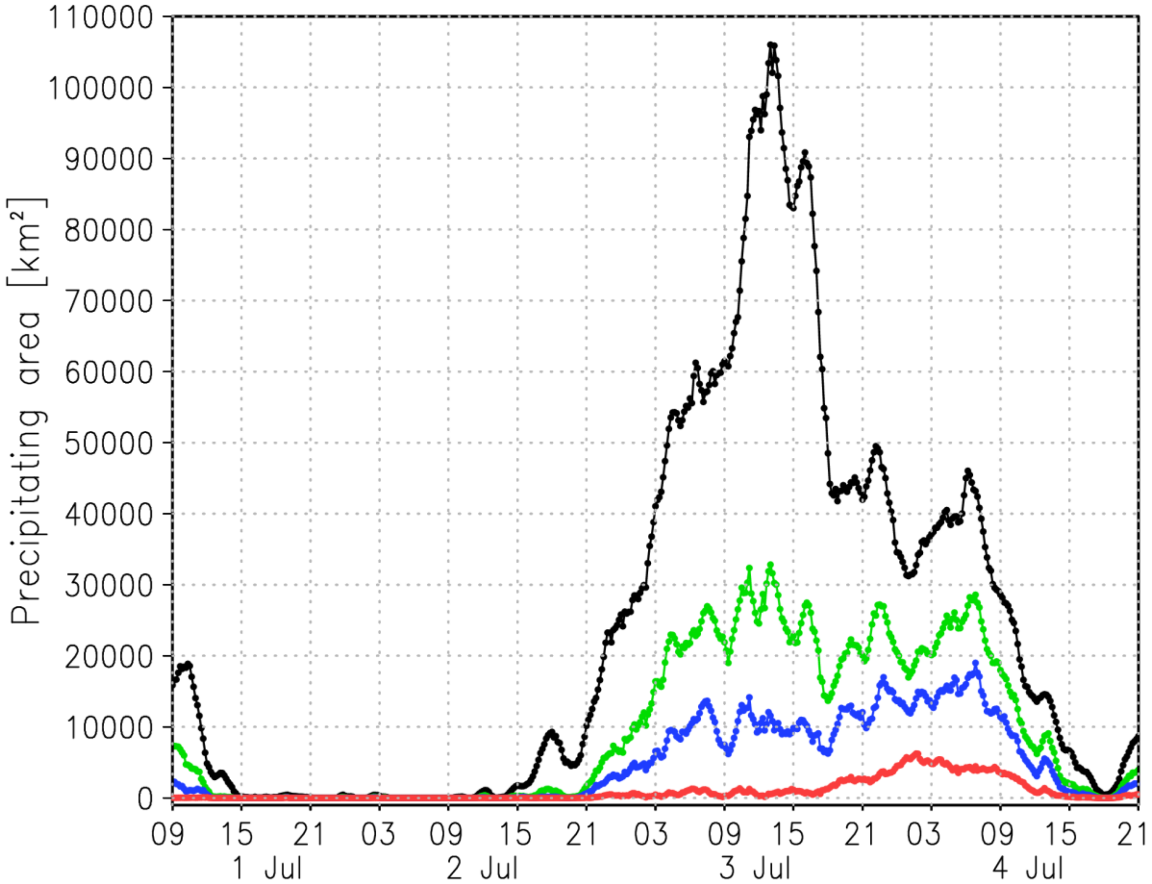

Fig. 4 (a) Time evolution of area coverages of precipitation (km^2) more than 1 mm h^{-1} (black), 5 mm h^{-1} (green), 10 mm h^{-1} (blue), and 30 mm h^{-1} (red) within the Kyushu area calculated with JMA operational radar data. The abscissa designates local time (UTC + 9).

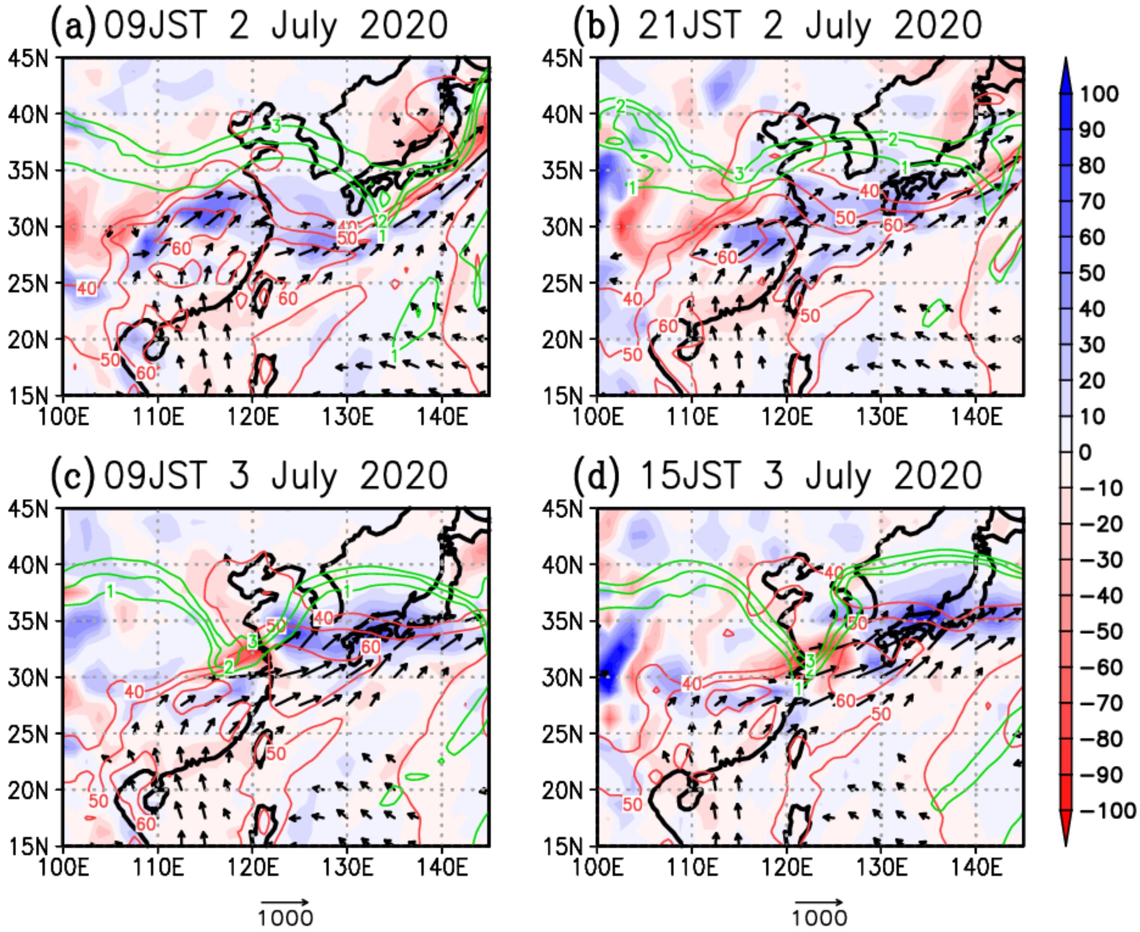

Fig. 5 Horizontal distributions of the free-tropospheric IVFC (color, mm day^{-1}), precipitable water (red contour, mm, shown only over 40 mm), free-tropospheric moisture flux (vector, kg m^{-1} s^{-1}, shown only over 200 kg m^{-1} s^{-1}), and isentropic potential vorticity on 350 K (green contour, shown only 1, 2, and 3 PVU) obtained from JRA55 data at (a) 09 JST 2 July, (b) 21 JST 2 July, (c) 09 JST 3 July, and (d) 15 JST 3 July.

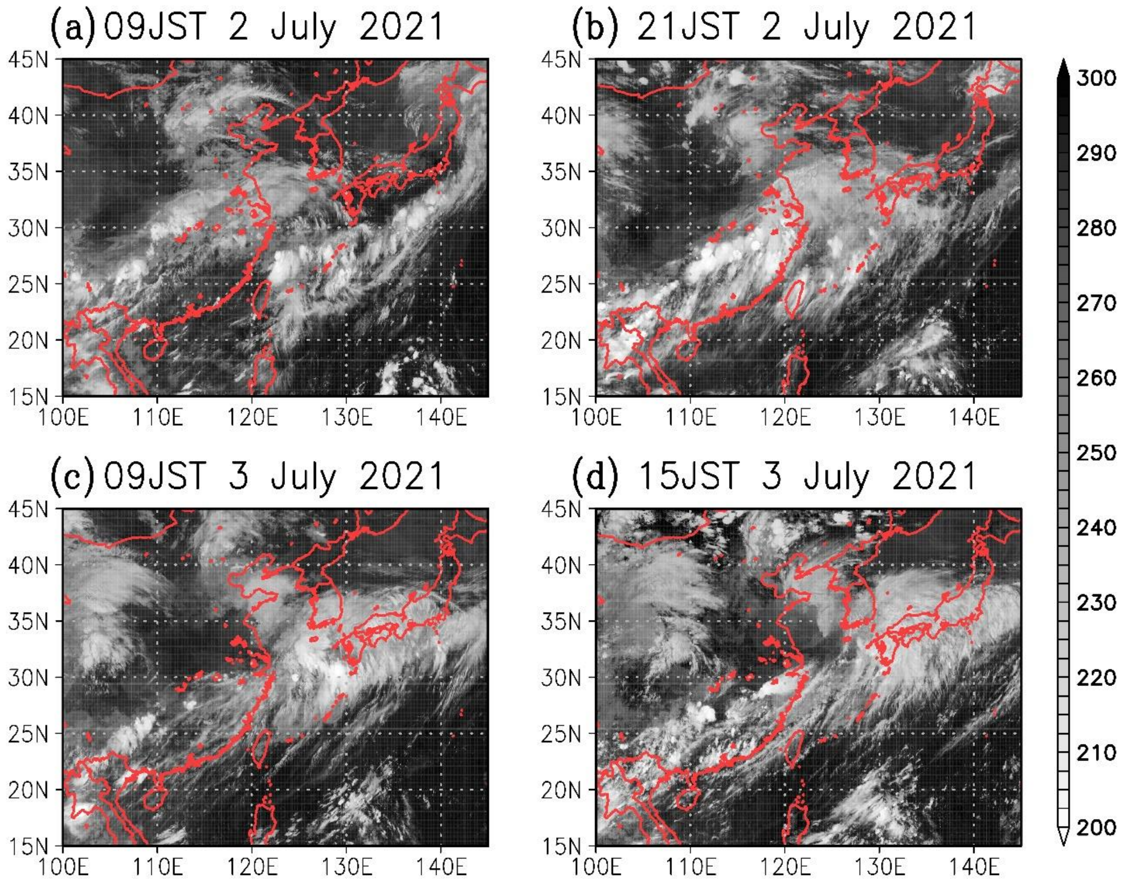

Fig. 6 (a) Infrared brightness temperature (K) observed by Himawari 8 at (a) 09 JST 2 July, (b) 21 JST 2 July, (c) 09JST 3 July, and (d) 15 JST 3 July.

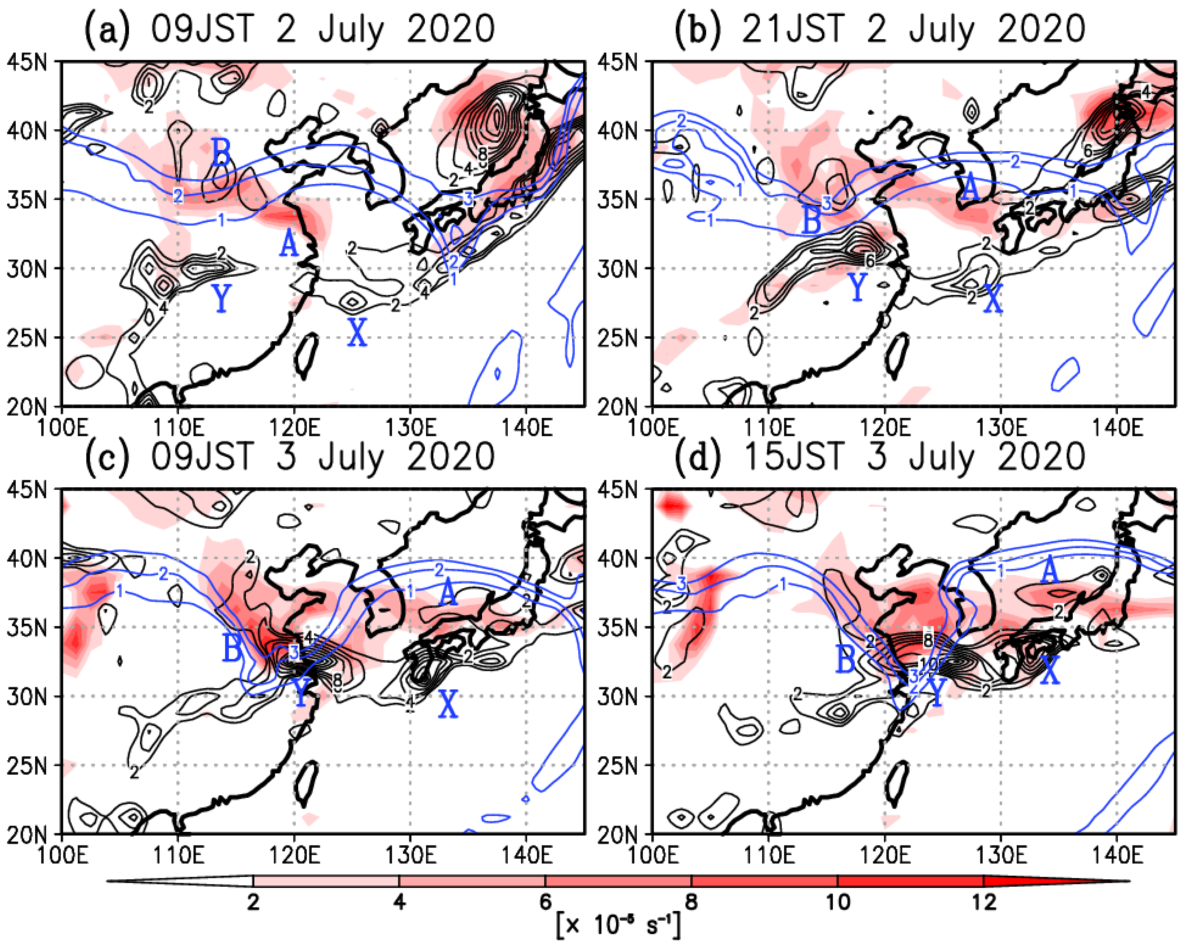

Fig. 7 Relative vorticity at 500 hPa (color, $\times 10^{-5}$ s^{-1}) and 850 hPa (black contours, $\times 10^{-5}$ s^{-1}) obtained from JRA55 data at (a) 09 JST 2 July, (b) 21 JST 2 July, (c) 09 JST 3 July, and (d) 15 JST 3 July. Only positive values are shown. Blue contours designate potential vorticity on 350 K isentropic surface (PVU, shown only 1, 2, and 3 PVU contours).

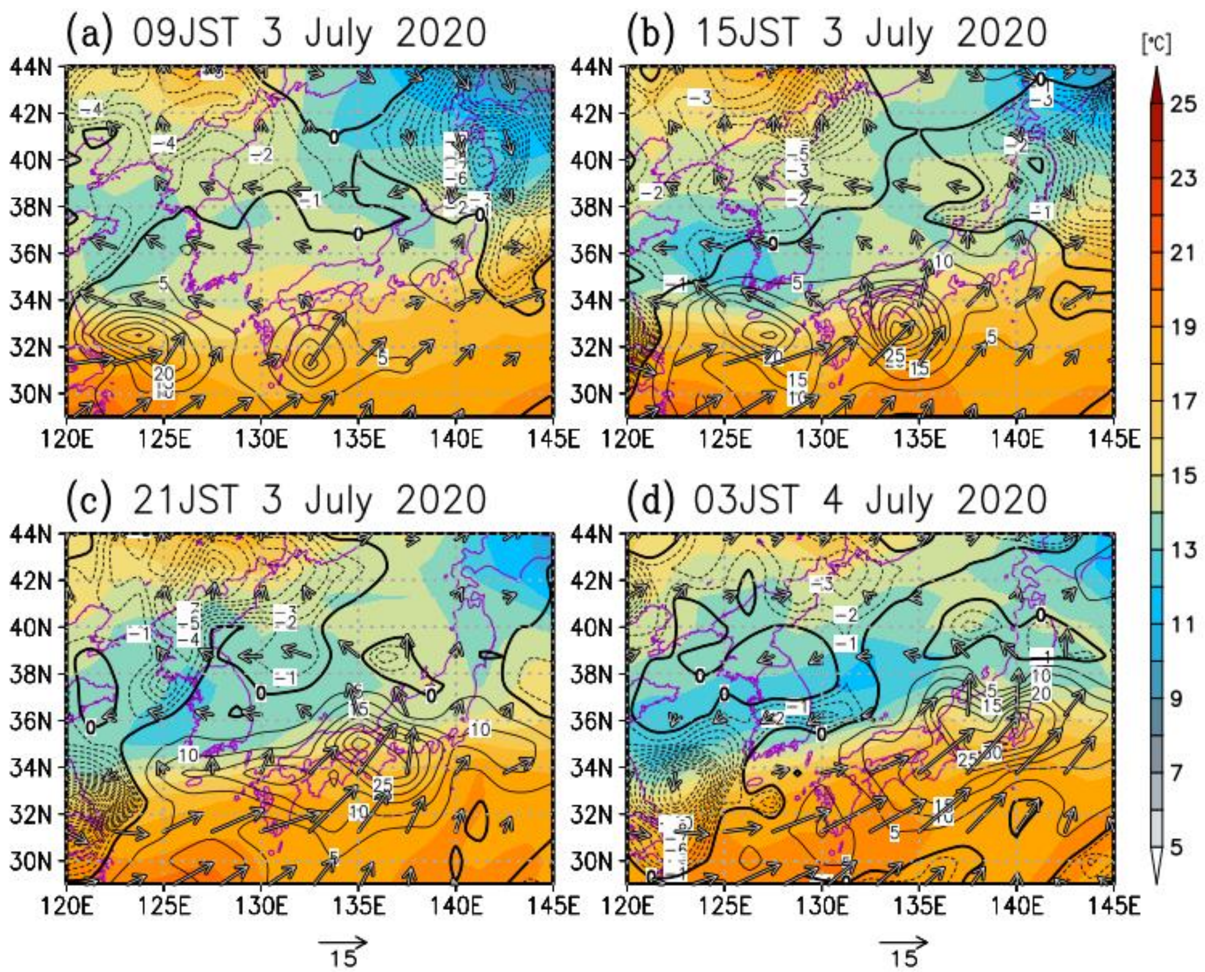

Fig. 8 Temperature (color, °C), wind vectors (m s^{-1}, shown only over 2.5 m s^{-1}), and horizontal temperature advection (contours, $-V \cdot \nabla T$, 10^{-5} K s^{-1}) at 850 hPa obtained from JRA55 data at (a) 09 JST 3 July, (b) 15 JST 3 July, (c) 21 JST 3 July, and (d) 03 JST 4 July. The contour intervals are 1×10^{-5} K s^{-1} for the cold advection and 5×10^{-5} K s^{-1} for the warm advection.

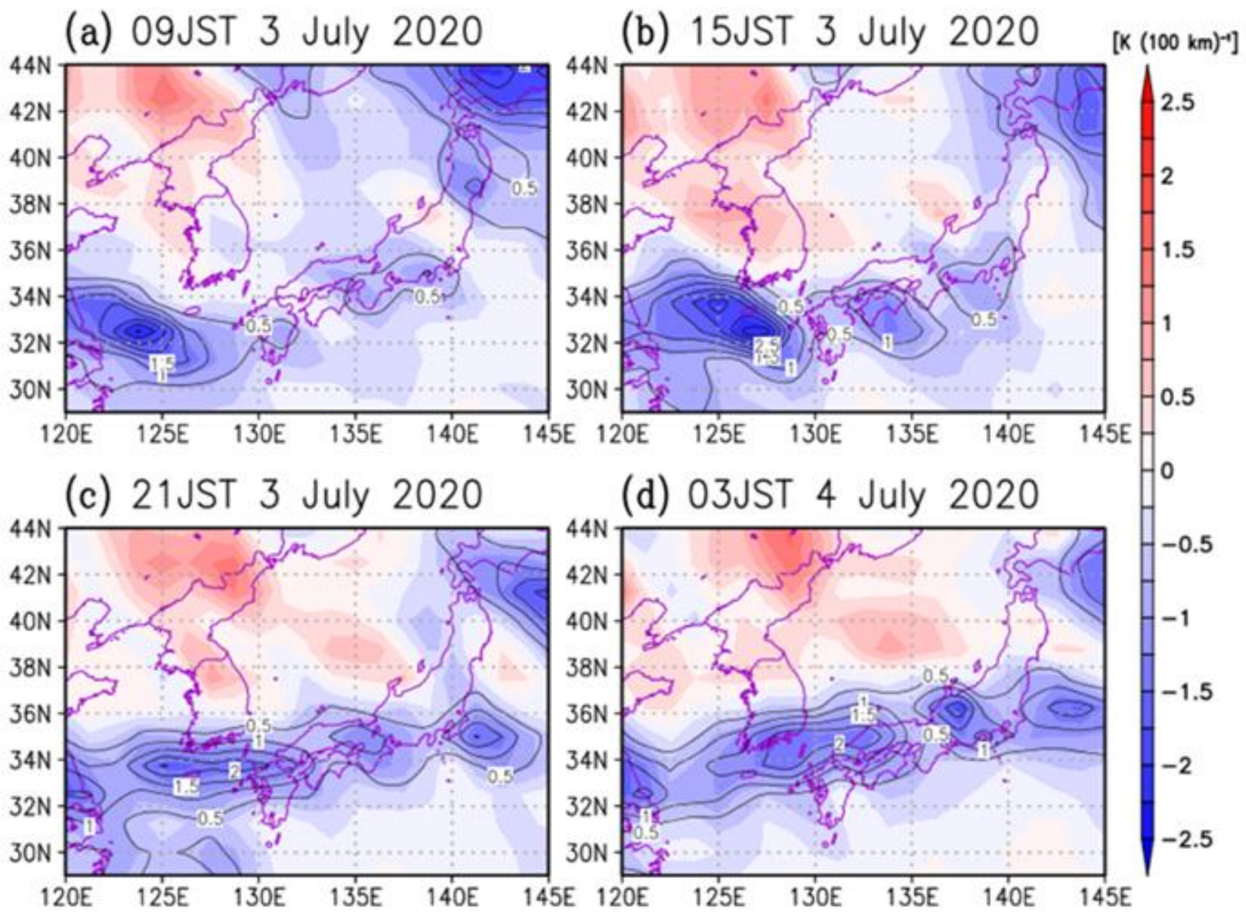

Fig. 9 Horizontal temperature gradient [color, K (100 km)$^{-1}$] and horizontal frontogenesis [K (100 km)$^{-1}$ (day)$^{-1}$, shown only over 0.5 K (100 km)$^{-1}$ (day)$^{-1}$] at 850 hPa calculated with JRA55 data at (a) 09 JST 3 July, (b) 15 JST 3 July, (c) 21 JST 3 July, and (d) 03 JST 4 July.

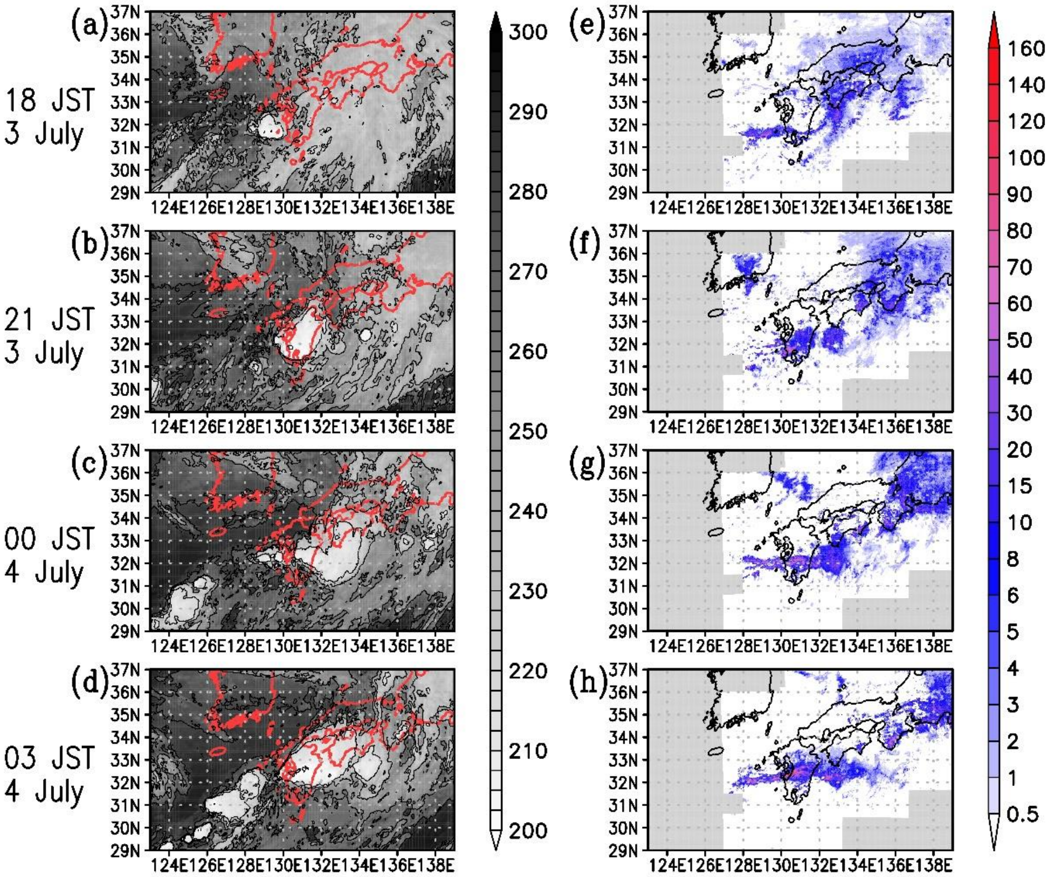

Fig. 10 (a–d) Infrared brightness temperature (K) observed by Himawari 8 and (e–h) precipitation distribution observed by JMA weather radar (mm h^{-1}) at (a, e) 18 JST 3 July, (b, f) 21 JST 3 July, (c, g) 00 JST 4 July, and (d, h) 03 JST 4 July.

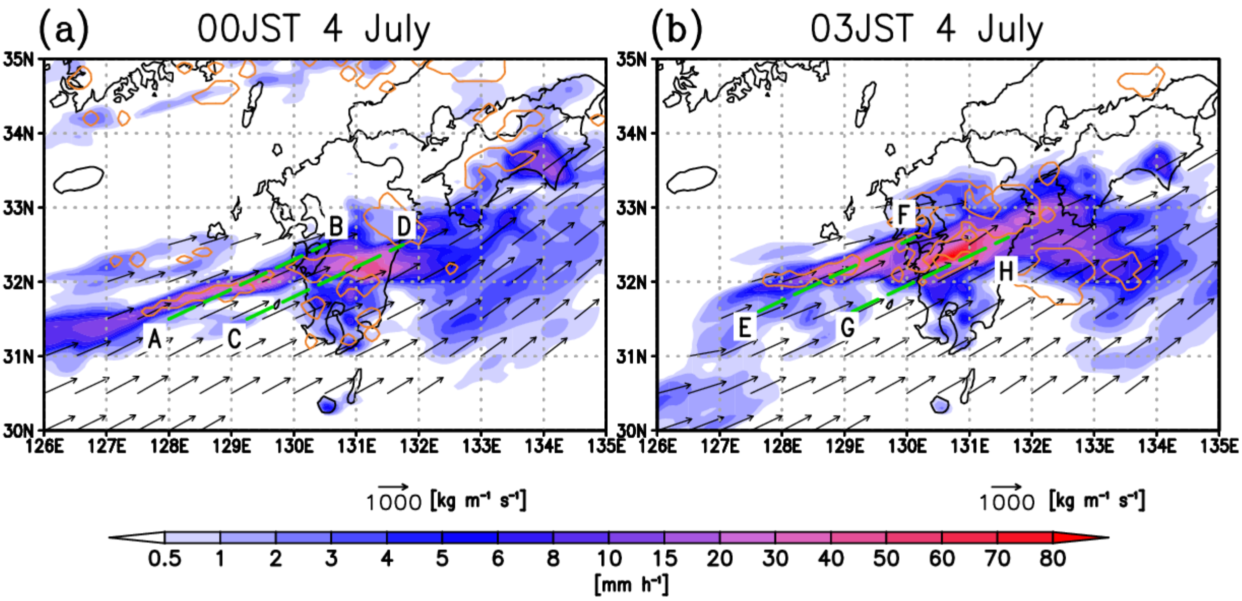

Fig. 11 Precipitation distribution (color, mm h^{-1}) and vertically (1000–300 hPa) integrated water vapor flux (vector, kg m^{-1} s^{-1}, shown only over 1000 kg m^{-1} s^{-1}) obtained from the MSM data at (a) at 00 JST 4 July and (b) 03 JST 4 July. Orange contours designate areas where MAUL conditions are satisfied at least 2 vertical levels between 500 and 800 hPa. Green dashed lines mark the location of the cross-sectional analyses in Fig. 12.

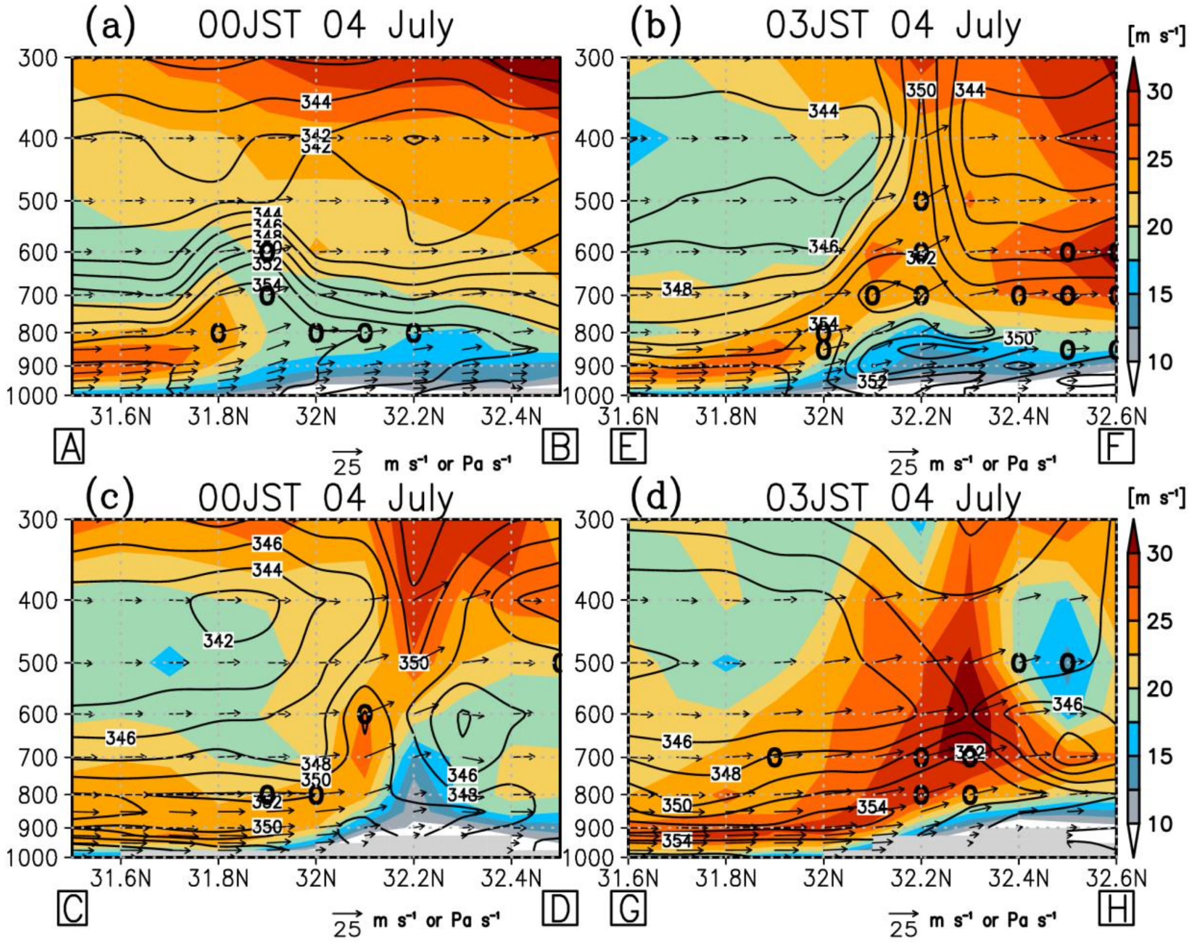

Fig. 12 Vertical cross-sections of a wind velocity along the cross-section (color, m s^{-1}), wind vectors (arrow, m s^{-1} for horizontal direction and Pa s^{-1} for vertical direction), and equivalent potential temperature (black contour, K) along the green dashed lines in Fig. 10 at (a, c) 00 JST 4 July and (b, d) 03 JST 4 July. The black circles indicate grids that fulfill the MAUL condition. The ordinate designates pressure (hPa).

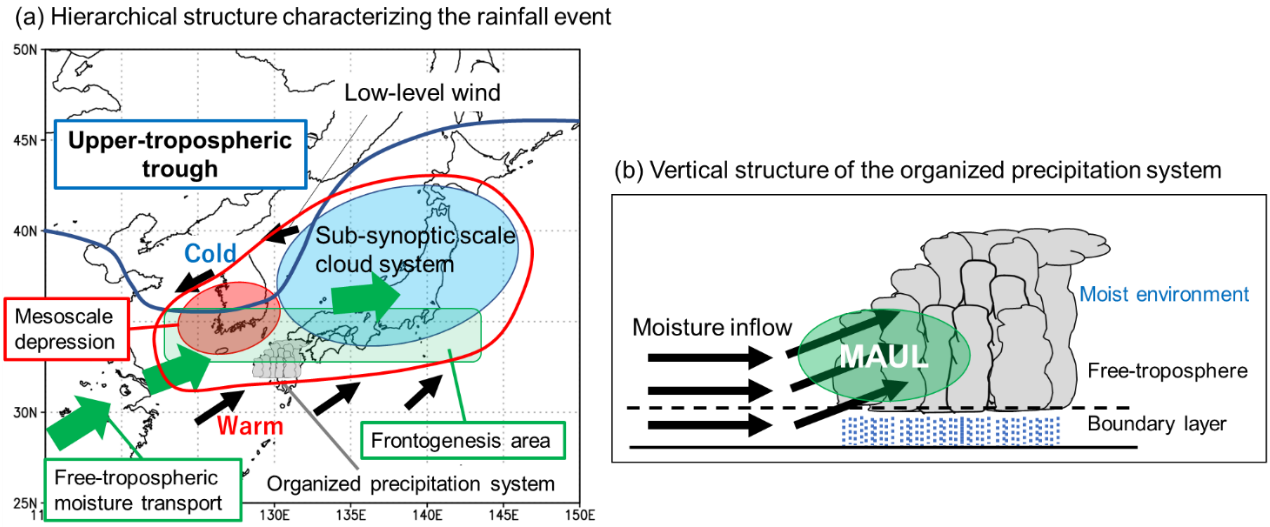

Fig. 13 Schematics of (a) the hierarchical structure characterizing the heavy rainfall event, and (b) Vertical structure of the organized precipitation system. Note that MAUL designate moist absolutely unstable layer.